

- **Title:** *Damage Quantification of Intact Rocks Using Acoustic Emission Energies Recorded During Uniaxial Compression Test and Discrete Element Modeling*<sup>1</sup>

• **Author names and affiliations:**

- 1- **Cyrus Khazaei, PhD student (Corresponding Author)** <sup>1</sup>
- 2- **Jim Hazzard, PhD, PEng** <sup>2</sup>
- 3- **Rick Chalaturnyk, PhD, PEng** <sup>1</sup>

<sup>1</sup> NREF/CNRL Markin Bldg

Department of Civil and Environmental Engineering

University of Alberta

Edmonton, Alberta, Canada T6G 2W2

Em: [khazaei@ualberta.ca](mailto:khazaei@ualberta.ca)

Em: [rjchalaturnyk@ualberta.ca](mailto:rjchalaturnyk@ualberta.ca)

<sup>2</sup> Itasca Consulting Group Inc.

Toronto, Ontario, Canada M5C 1H6

Em: [jhazzard@itascacg.com](mailto:jhazzard@itascacg.com)

---

<sup>1</sup> This paper is originally published in Computers and Geotechnics <http://dx.doi.org/10.1016/j.compgeo.2015.02.012>

## Contents

Abstract.....	3
1. Introduction .....	3
2. Theory.....	5
3. Description of the Material and Experiment .....	6
3.1. Analysis of the Experimental Data .....	9
4. Numerical Model .....	13
4.1. Algorithm for Recording AE Events.....	14
4.2. Results.....	15
5. Discussion .....	20
6. Conclusion.....	23
Acknowledgement.....	24
References.....	25

## Abstract

In this paper, acoustic emission (AE) energies recorded during 73 uniaxial compression tests on weak to very strong rock specimens have been analyzed by looking at the variations in b-values, total recorded acoustic energy and the maximum recorded energy for each test.

Using 3D Particle Flow Code (PFC3D), uniaxial compression tests have been conducted on discrete element models of rocks with various strength and stiffness properties. An algorithm has also been used to record the AE data in PFC3D models based on the change in strain energy upon each bond breakage.

The relation between the total released acoustic energy and total consumed energy by the specimens has been studied both for the real data and numerical models and as a result, a linear correlation is suggested between the released AE energy per volume and consumed energy per volume of the intact rocks.

Comparing the recorded acoustic energies in numerical models with real data, suggestions are made for getting realistic AE magnitudes due to bond breakages (cracks) from PFC3D models by proposing a modification on Gutenberg-Richter formula that has been originally proposed for large scale shear induced earthquakes along faults.

Also, using the numerical model, an attempt has been made to quantify the damage to the intact rock by proposing a damage parameter defined as the total crack surface observed during the tests divided by the total crack surface possible based on size of particles.

**Keywords:** Acoustic Emission, Uniaxial Compression Test, Intact Rock, Damage Quantification, Particle Flow Code (PFC3D)

## 1. Introduction

It is known that the damage process of intact rocks starts with tensile cracks growing parallel to the maximum principal stress until a “critical crack density” is reached and a “process zone” is formed [Reches & Lockner, 1994; Scholz, 1968]. This manifests with reduction in cohesion during development and coalescence of cracks until a dominantly frictional rupture occurs along the formed shear band and the specimen fails [Lockner et al., 1991; Martin & Chandler, 1994]. A technique to observe the damage process of rocks is acoustic emission (AE)

monitoring. Acoustic emission is defined as an elastic wave propagated due to a rapid release of energy within the material [Lockner, 1993]. Analyzing the waveforms and using techniques such as Seismic Moment Tensor Inversion (SMTI), source locations as well as the mechanism of events can be identified [Kishi et al., 2000].

There have been many attempts to correlate the observed AE activity with the stress level or different stages of rupture in geo-materials. It is known that there is an overall correlation between the evolution of stress strain curve in rocks and the AE rate [Eberhardt et al., 1999; Scholz, 1968]. Therefore, the simplest technique would be to correlate the number of events with the observed mechanical behavior [Koerner & Lord, 1984; Ohnaka & Mogi, 1982; Seto et al., 2002]. However, it has been suggested that instead of cumulative number of events, the cumulative AE energy would be physically more meaningful [Ganne et al., 2007; Přikryl et al., 2003; Yukalov et al., 2004].

Although there have been several studies on the AE behavior of granular soils [Hill et al., 1998; Koerner et al., 1977, 1981], clays [Koerner et al., 1977; Lavrov et al., 2002; Thoeny et al., 2010], soft rocks such as Tuff and Shale [Amann et al., 2011; Fujii et al., 2009; Hall et al., 2006; Mito et al., 2007; Mori et al., 2007; Niandou et al., 1997; Valès et al., 2004] and hard rocks mostly granite [Cox & Meredith, 1993; Sellers et al., 2003; Sondergeld & Estey, 1981; Zang et al., 2000], the literature review reveals that there is an absence of reports on the variations of released energies specially for weak rocks. The main reason is probably the high attenuation of such material and the fact that many events are too small to trigger the sensors. Also, the majority of AE studies in rock materials are devoted to hard rocks while new applications of AE monitoring especially in Petroleum engineering require understanding of the release of AE energy in weaker classes of rocks.

Therefore, in this paper a wide range of rocks with different strength and stiffness properties have been studied with the purpose of understanding the relation between the amounts of released acoustic energy with the total consumed energy. Also, using discrete element modeling, an attempt has been made to quantify the amount of damage in terms of crack surface for the materials studied.

## 2. Theory

Any extra energy put into a system, ex. intact rock, which is already in a state of equilibrium, has to somehow dissipate so that the system regains its stable equilibrium by reaching its minimum potential energy. This decrease in potential energy to reach the equilibrium state is achieved by continuous lengthening of cracks passing the rock from unbroken to broken condition [Griffith et al., 1997; Griffith, 1921]. The dissipation of energy can be in various forms such as propagation of cracks or acoustic waves.

Figure 1 shows the stress-deformation curve for an arbitrary rock. The area under the loading curve (solid line),  $A(\Delta OAB)$ , is the extra energy put into the system. Two possible response curves of the rock are shown with dotted lines. The area under these two curves,  $A(\Delta OAE)$  and  $A(\Delta OAD)$ , would be the energy required to extend the cracks.

If  $A(\Delta OAB) < A(\Delta OAD)$  which is the case for a ductile rock with smaller Young's modulus, the crack will not propagate but it is possible that it undergoes some form of time-dependent weakening due to various phenomena such as flow of fluid to the crack that in turn result in reduction of the energy required to extend the crack (shifting the curve AD toward AB). In this case, although there is no excess energy yet to produce seismicity, the crack can still propagate (aseismic deformation) [Fairhurst, 2013]. If  $A(\Delta OAB) > A(\Delta OAE)$  which is the case for a brittle rock with higher Young's modulus, the excess energy shown as the shaded area contributes to acceleration of cracks and release of seismic energy.

Figure 1 is a simplified demonstration of how ductility contributes to the extent of AE energy with the rock being loaded elastically until point A and seismic energy released during the unloading after point A. In practice, AE events have been observed as early as the crack initiation strength (~40-60% of the peak strength) is reached [Cai et al., 2007; Cai, 2010].

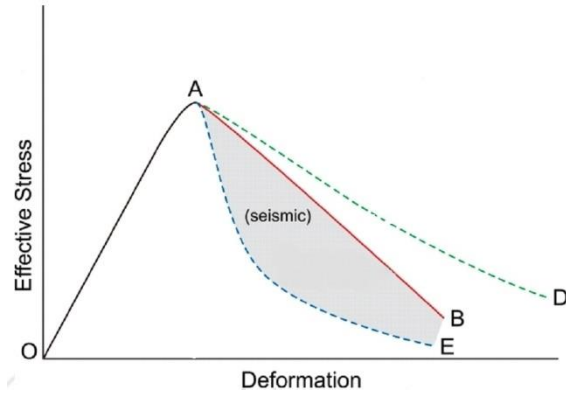


**Figure 1: Schematic load-deformation curve for an intact rock. OAE and OAD curves are response curves for a brittle and ductile rock, respectively. Shaded area is the excess energy released as acoustic emission (modified after [Fairhurst, 2013])**

### 3. Description of the Material and Experiment

“Intact rock” in engineering terms is referred to the rocks with no significant fractures [Harrison & Hudson, 2000]. In order to understand how the intact rocks responds acoustically, a large database of laboratory tests reported by CANMET conducted as a part of low and intermediate level radioactive waste Deep Geologic Repository (DGR) design for the Ontario Power Generation (OPG) is analyzed in this paper. The repository is located within the sedimentary bedrock beneath the Bruce site near Kincardine, Ontario at about 660 m depth [Gorski et al., 2009a]. The Precambrian Granite basement of the site at 860 m is overlain by flat lying Palaeozoic age dolostone, shale and limestone sedimentary rocks. A review of the geomechanical properties of the rocks in DGR excavations is presented by [Lam et al., 2007].

A total number of 73 uniaxial tests were conducted on specimens of shale, limestone and dolostone rocks with acoustic emissions being monitored during the tests. Although an abrupt shift in stress-strain curves has been observed for some specimens indicating the existence of planes of weakness that caused failure [Gorski et al., 2009a] and questioning the “intact” nature of them, due to the small size of laboratory specimens, it is assumed that the majority of specimens have been intact and therefore the observed AE response would belong to the intact rock. According to the results, several rock units were identified based on ASTM D5878 [ASTM, 2005]. The rocks have also been classified according to ISRM classification [Brown, 1981] (Figure 2). The classifications are summarized in Table 1.

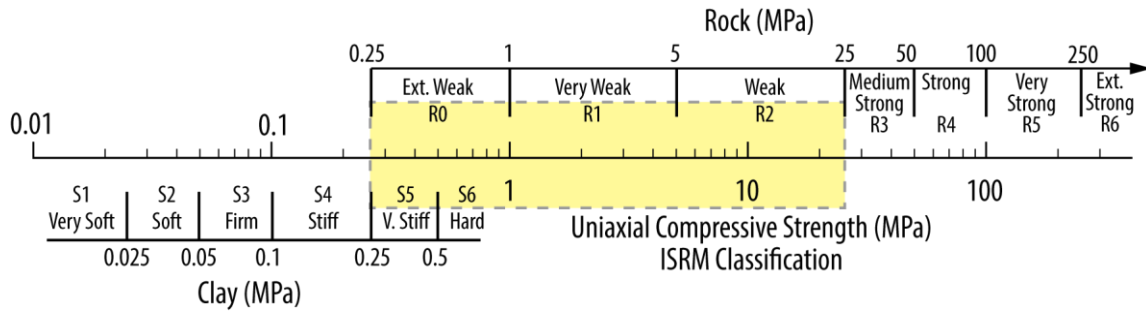


**Figure 2: ISRM classification of rocks based on uniaxial compressive strength**

**Table 1: Rock types identified by CANMET [Gorski et al., 2009a]**

Rock Type	Description	ISRM Class	UCS (MPa)
brecciated dolostone	weak	R1-R2	5-25
dolomitic shale	medium strong	R3	25-50
shale	medium strong	R3	25-50
shale with limestone layers	medium strong	R3	25-50
limestone with shale layers	medium strong	R3	25-50
dolostone	strong	R4	50-100
argillaceous limestone	very strong	R5	100-250
crystalline dolostone	very strong	R5	100-250

The specimens showed a wide range of compressive strengths from 1 to 200 MPa and Young's moduli from 0.5 to 60 GPa as shown in Figure 3.

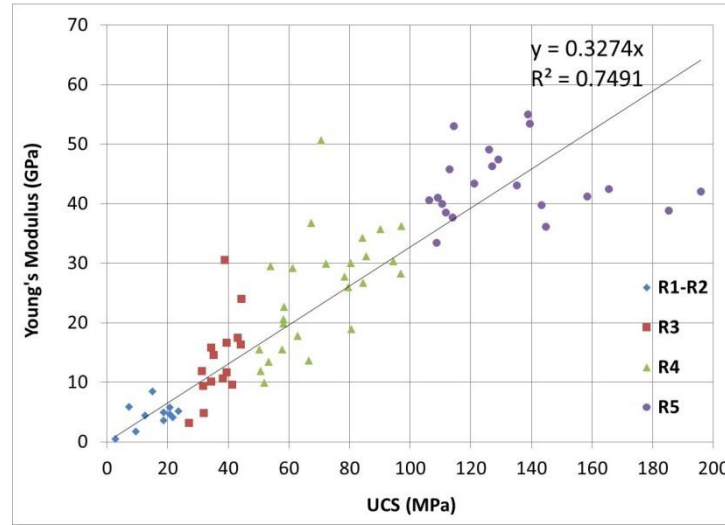


**Figure 3: Young's modulus versus unconfined compressive strength for the specimens tested by CANMET (data is color coded according to the ISRM classification)**

The specimens had an average length and diameter of 176 mm and 74 mm, respectively. The loading in uniaxial compression tests was conducted in stress controlled manner to imminent failure at the rate of 0.75 MPa/s based on ASTM D7012 [ASTM, 2007]. The AE recording system consisted of 12 transducer channels, 16 bit, 10 MHz, 40 dB preamplification, 60 dB gain, high and low pass filters and source location software. Two arrays of 3 piezoelectric sensors were mounted on the outer surface at the top and bottom halves of each specimen. The sensors on each array were 120° apart.

AEWin software was used to record the AE data in the lab. Since the outputs of this software will be used for analyses in the next sections, it is necessary to describe what the recorded energies by AEWIn signify. The reported energies by CANMET are “Absolute Energy”. This energy is based on the sum of squared voltage readings divided by a token resistance R, as explained by Pollock [Pollock, 2013] and shown in Equation (1):

$$U = \frac{1}{R} \sum_{FTC}^{PDT} V_i^2 \cdot \Delta t \quad (1)$$

where R is equal to 10 kΩ representing the input impedance of the preamplifier, FTC stands for “First Threshold Crossing” and PDT stands for “Peak Definition Time”. The energies were

reported in attojoules ( $\text{aJ}=10^{-18}$  J). This “Absolute Energy” is a good feature to deal with larger signals resulting from burst type emissions [Pollock, 2013].

Although since the events have a very high frequency and it is likely that there has been spreading/attenuation even on the small scale of tested specimens, due to lack of source location data, in this research it is assumed that the energy is non-dispersive and therefore, the energies recorded at the sensors are equal to the released energies at the source. Thus, without any further corrections to consider signal loss due to attenuation, having the released energy, magnitude of an AE event can be calculated by the empirical Equation (2) [Scholz, 2002]:

$$M_e = \frac{2}{3} \log E - 3.2 \quad (2)$$

where  $E$  is the energy in Joules.

### 3.1. Analysis of the Experimental Data

In order to study the variations of AE behavior in different rocks, various items such as b-value, maximum released energy during the test, total released AE energy and total consumed energy by the specimen have been investigated in this section.

A parameter often used in seismic studies is b-value defined by the Gutenberg-Richter relationship as shown in Equation (3) [Gutenberg & Richter, 1954]:

$$\log N = a - bM \quad (3)$$

where  $N$  is the number of AE events greater than the magnitude  $M$ . The b-value represents a statistical distribution of magnitudes [Manthei et al., 2000]. A large b-value indicates larger proportion of small events. Variations of b-values with uniaxial compression strength (UCS) are shown in Figure 4.

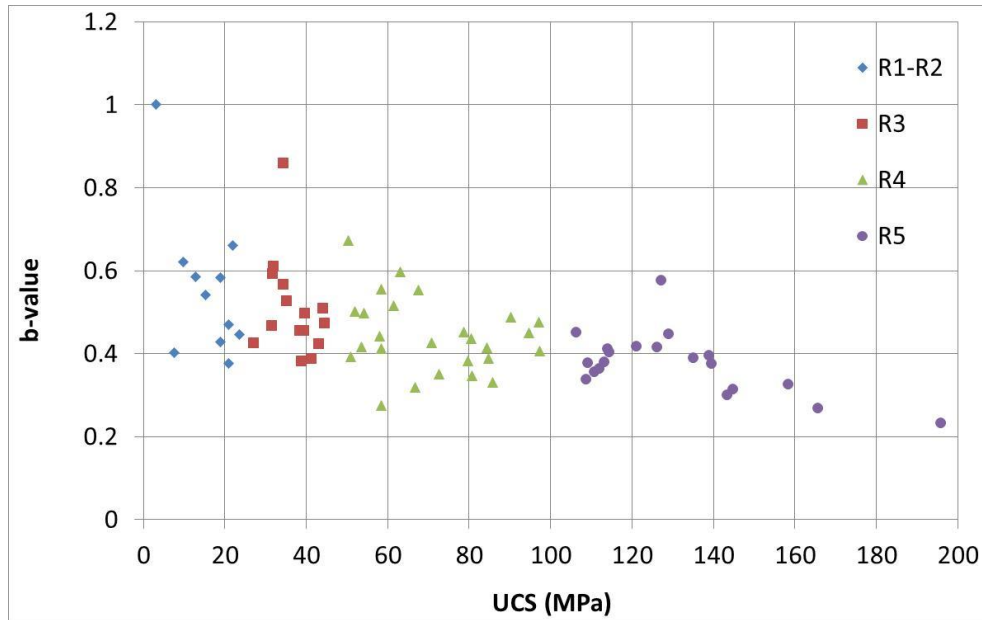


**Figure 4: Variations of b-values obtained for DGR-1, DGR-2 and DGR-3 tests conducted by CANMET versus unconfined compressive strength**

As expected, a slight reduction in b-values is observed for stronger rocks indicating dominance of larger magnitude events in them. In other words, larger b-values in weaker rocks indicate the abundance of smaller scale events. However, b-values do not provide any info on the range of energy release in each class of rocks. Therefore, in order to investigate the greatest amount of energy release (the largest magnitude) expected from a certain type of rock, variations of the maximum recorded energy in each test versus UCS are also plotted in Figure 5.

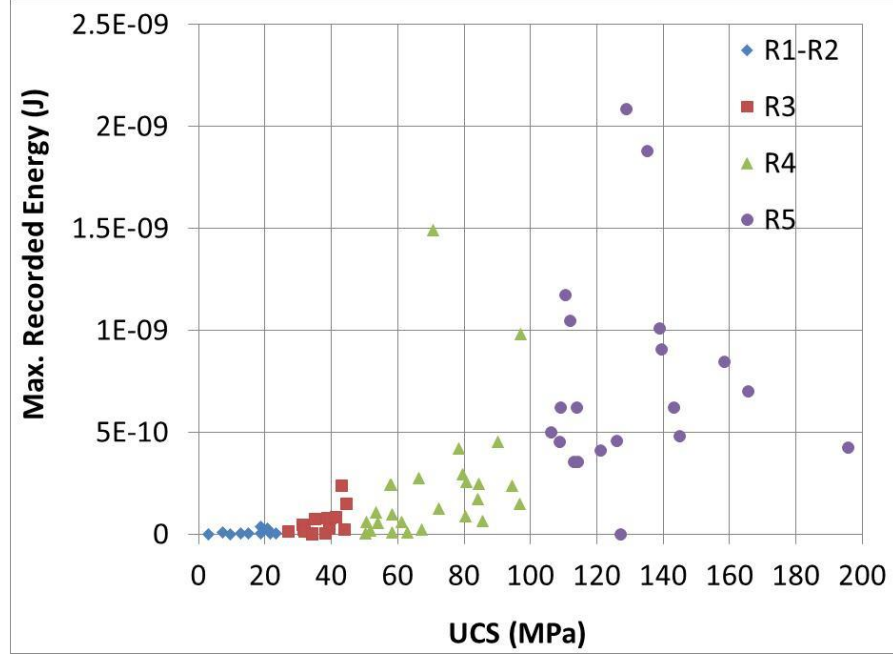


**Figure 5: The maximum energy release versus the UCS**

According to this Figure and using Equation (2), the largest magnitudes recorded for all the specimens in uniaxial compression tests are almost in the range of -9 to -10.

On the other hand, the damage process usually involves the emission of hundreds of events and thus, the relation between the total consumed energy by the specimen and total released acoustic energy is also studied. The stress-strain plots reported by CANMET show that most of the tests have been stopped almost right after the peak strength was reached [Gorski et al., 2009a, 2009b]. Also, it is known that the stress-strain curve of rocks has a non-linear part at the beginning due to closure of cracks and a non-linear part prior to the peak stress. However, the consumed energy by each specimen is estimated considering a linear curve from the start up to the peak stress and therefore, using the peak compressive strength (UCS) and its corresponding strain, the total energy consumed by the specimen per unit volume is estimated by Equation (4) and plotted versus the total recorded acoustic energy divided by the volume of each specimen in Figure 6.

$$W_{cons.} = \sum (\sigma \times \Delta \varepsilon) \approx \left[ \frac{\sigma_p \times \varepsilon_p}{2} \right] \quad (4)$$

where  $W_{cons.}$  is in  $\frac{N.m}{m^3}$  (also Joules/m<sup>3</sup>),  $\Delta\varepsilon$  is the strain increment,  $\sigma_p$  is the unconfined compressive strength of the specimen in Pa and  $\varepsilon_p$  is the strain corresponding to  $\sigma_p$ .

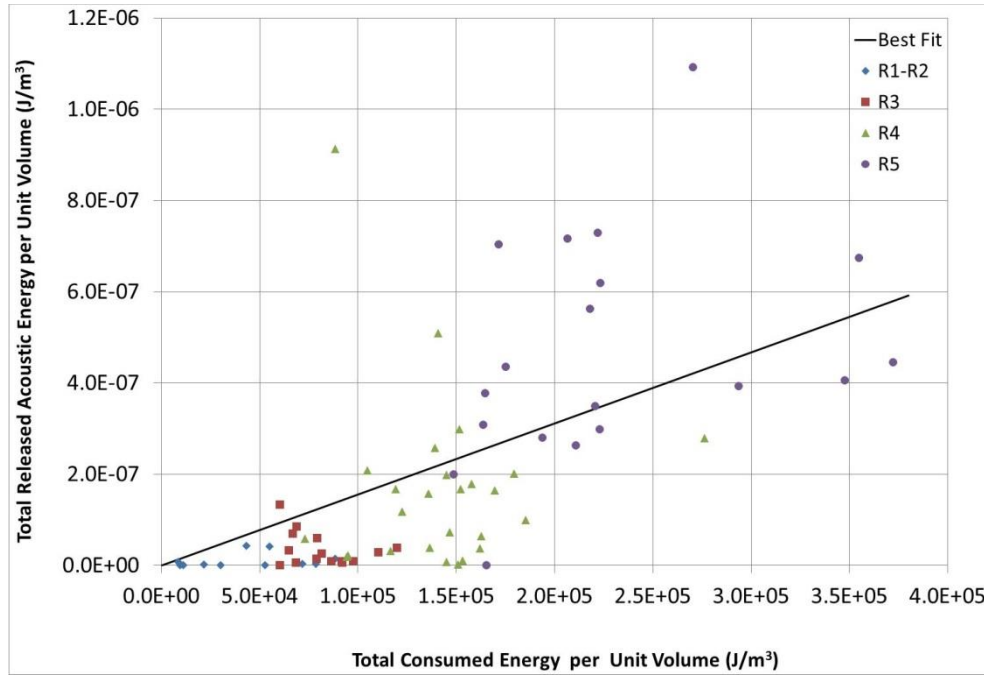


**Figure 6: Variations of the total recorded acoustic energy versus the total consumed energy by the specimen**

As can be observed in this Figure, there is a large discrepancy amongst the data and although there seems to be a power law correlation between the x and y values, a linear fit would result in a higher  $R^2$  and also for the sake of simplicity, a linear fit has been applied to the data as shown in Equation (5) (adjusted  $R^2=0.62$ ):

$$E_{UCT} = (1.56 \times 10^{-12}) W_{UCT} \quad (5)$$

where  $E_{UTC}$  is the sum of all recorded AE energies during the test divided by the volume of each specimen and  $W_{UTC}$  is the total energy consumed per volume of the specimen calculated using Equation (4).

## 4. Numerical Model

Discrete element modeling allows detailed observation of the changes in energy as damage occurs within the rock specimen. In this study, Particle Flow Code, PFC3D v5.0 (Itasca Consulting Group, 2014), has been used to model uniaxial compression tests on specimens with the same size as those tested by CANMET.

In a PFC3D model, the rock matrix is generally idealized with a group of particles bonded together by models such as parallel bond model [Potyondy & Cundall, 2004]. Size distribution of particles allows modeling the geometrical heterogeneity which is an advantage compared to continuum models. The particles are rigid and the bonds can only break apart in tension or shear (there is no particle breakage).

The micro parameters of parallel bonds are calibrated in a trial and error process where the micro-parameters are changed until the desired macro-response is observed. In this research, the models have been calibrated for a range of uniaxial compressive strengths and Young's moduli based on the data presented in Figure 3.

One technique to record stress-strain changes in PFC3D models is the use of "measurement spheres" that are representative volumes in which stress and strain are calculated. A complete formulation of how calculations are performed within a measurement sphere could be found in the PFC3D manual [Itasca, 1999].

Once the geometry of the model is generated and appropriate measurement spheres are installed, the load is applied to the model and then integrating twice the Newton's second law of motion, velocities and positions of all the particles are updated resulting in calculation of new contact forces with a force-displacement law. This cycle of calculating displacements and forces continues until a certain criterion is met [Itasca, 1999]. This process results in breakage of some bonds (cracks) that can be considered as AE events.

#### 4.1. Algorithm for Recording AE Events

A common method to record seismic magnitudes in PFC is by monitoring changes in forces around each new bond breakage within a certain distance and time and then calculating the moment tensors, scalar moment and moment magnitudes based on that [Hazzard & Young, 2000, 2002, 2004]. However, some studies suggest this approach may overestimate the magnitudes [Young et al., 2005].

Another approach proposed by [Hazzard & Damjanac, 2013] is to record the release of strain energy within a small volume around the newly formed cracks for a short period of time and then calculating the magnitudes using Equation (2). The change in energy would increase as the monitored volume increased and the appropriate volume would depend on the nature of cracking (e.g. tensile cracks in a compression regime or in a tensile regime) as well as location of events relative to the edge of the specimen [Damjanac, 2010].

A review of all techniques on how AE data can be obtained from PFC models is presented by [Hazzard & Damjanac, 2013]. According to that study, the latter algorithm based on energy changes is believed to provide more accurate magnitudes and is used in the present research.

In this algorithm, a “space window (small volume)” is monitored around each crack once it’s formed for a “time window” during of which the crack is “active”. If each bond breakage is considered as a single AE events, all the magnitudes will be close to each other which is not realistic and thus a common practice is to cluster the events in PFC models. In order to cluster the events, if a new crack is formed within the space window of a crack while the strain energy is still being monitored, the two cracks are considered part of one event, the time window is reset and the space window is expanded with regard to the new centroid of the event (that is now consisted of two particles). Otherwise, the crack is assumed part of a new event. The time and space windows of 40 steps and 2 average particle diameter, respectively, were suggested by [Hazzard & Damjanac, 2013] to provide realistic distribution of magnitudes and are used in this research too.

## 4.2. Results

Fifteen uniaxial compression tests have been conducted on cylindrical specimens generated by PFC3Dv5.0, the calibration of which is summarized in Table 2. Since the purpose of this research is to study the overall AE activity with regard to the strength properties, the calibrations do not represent any specific real specimens and instead, the UCS values are chosen only so that they cover the range of rocks similar to the real data. The Young's moduli are chosen based on Figure 3. The lengths and diameters of all the numerical specimens were equal to 176 mm and 37 mm, respectively.

**Table 2: Calibration parameters of PFC3D specimens. The average radius for all the models has been 2 mm (14043 particles). The coefficient of friction (ba\_fric) for all the specimens has been equal to 3.5 and the Young's modulus for all the balls has been set equal to the Young's modulus of parallel bonds (ba\_Ec=pb\_Ec).**

Rock	Macro Parameters		Micro Parameters (Parallel Bond Properties)		
	UCS (MPa)	Young's Modulus (GPa)	Young's Modulus pb_Ec (GPa)	Mean Normal Strength pb_sn_mean (MPa)	Standard Deviation of the Strength pb_sn_dev (MPa)
s1	21	5.9	5.4	14	3.8
s2	40	12.9	11.7	27	7.3
s3	41.7	13.7	12.5	28.6	7.8
s4	53.4	17.3	15.6	35.7	9.8
s5	61.5	21.3	19.5	44.6	12.3
s6	80.9	24.5	22.5	55	15
s7	84.3	27.8	25.7	58.7	16.2
s8	85	26.7	24.4	55.8	15.4
s9	95.4	32.2	30	66	18.2
s10	99.6	33.3	30.5	69.7	19.2
s11	108.6	35.3	32.5	74.2	20.4
s12	112.2	40.2	36.5	83.4	23
s13	123.9	41.6	38.1	87.2	24
s14	143.5	46.4	42.9	98.1	27
s15	158	52.5	47.7	109	30

The microseismic recording algorithm has been initiated once the loading started for each test. Three measurement spheres have been installed along the height of each specimen and stress strain response has been monitored for each measurement sphere throughout the test. The tests

have been stopped once the average stress was dropped to 20% of the peak stress. This threshold was chosen to capture the post peak behavior as well although the lab tests by CANMET were stopped almost right after the peak. The total consumed energy by the specimen was estimated as the sum of the area under these 3 stress-strain curves. As an example, one specimen is shown in Figure 7 along with the measurement spheres and recorded stress-strain curves.

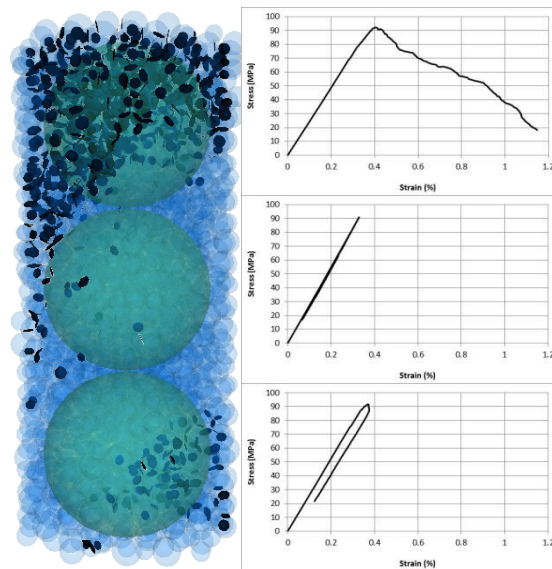


**Figure 7: A sample test with particles (blue), measurement spheres (green) and bond breakages (black) as well as stress-strain curves for each measurement sphere. Calibration would be based on UCS and Young's modulus from an average value obtained from the three measurement spheres with functions already available in PFC3D routines library**

As can be observed in this Figure, there is a correspondence between the absorbed energy by each section and the bond breakages as well as the AE released energy. Variations of the total released acoustic energy versus total consumed energy by each specimen are plotted in Figure 8.

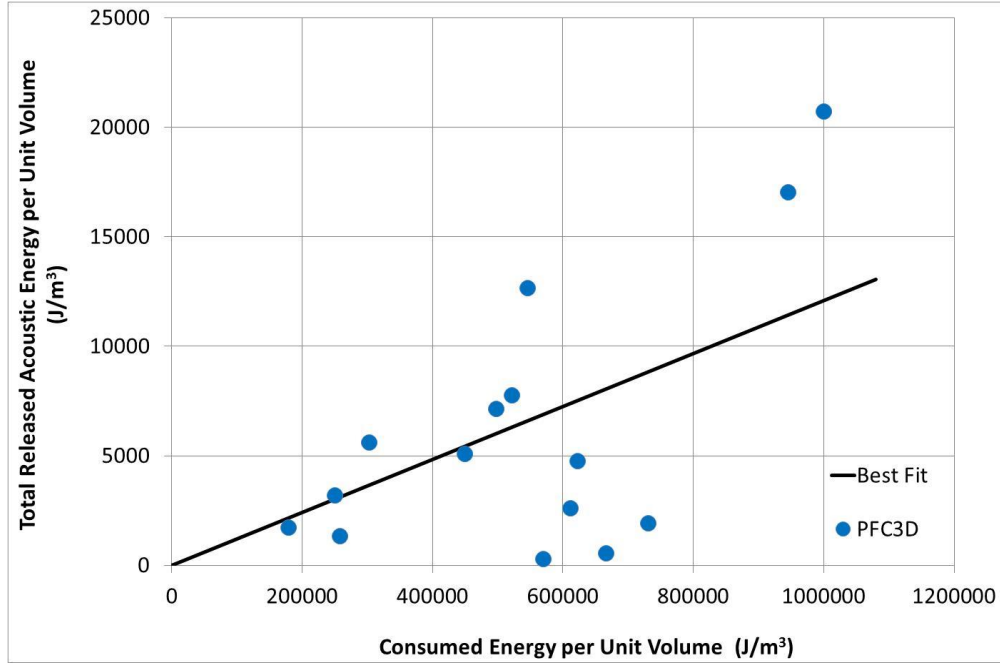


**Figure 8: Variations of the Released Acoustic Energy versus the Total Consumed energy**

According to this Figure, following correlation exists between the AE energies recorded by PFC3D and total consumed energy by each specimen (adjusted  $R^2=0.67$ ):

$$E_{PFC3D} = (1.21 \times 10^{-2}) W_{PFC3D} \quad (6)$$

Assuming the consumed energies by numerical models and real specimens are equal,  $W_{UCT} = W_{PFC3D}$ , and substituting  $W_{PFC3D}$  from Equation (6) into Equation (5), a correlation between real AE energies and numerical AE energies is obtained as following:

$$E_{UCT} = (1.29 \times 10^{-10}) E_{PFC3D} \quad (7)$$

This is actually reasonable since all the events are not recorded in the lab due to various practical limitations but in a PFC model, all the events are recorded and therefore the energy would never balance. Substituting the real energy,  $E_{UCT}$ , from Equation (7) into Equation (2), a modified form of Gutenberg-Richter equation is obtained that would work for the AE events in PFC3D models:

$$M_e = \frac{2}{3} \log E_{PFC3D} - 9.8 \quad (8)$$

In order to have a real estimate of the extent of cracking at each level and its correspondence with the AE data and consumed energy, it would be required to: a) Use techniques such as X-ray tomography on samples of failed specimens to have an estimate of the crack length/surface [Elaqra et al., 2007; Suzuki et al., 2010; Watanabe et al., 2004] b) Have the location and energy of AE events and c) Use local stress-strain measurements along the height of specimens to have an estimate of the consumed energy at each level. Unfortunately, there has been no X-ray tomography and local stress-strain measurements for the data analyzed in this research and except the recorded energies; the quality of the source location data is not good enough for further analyses. However, it was hoped that the numerical model could provide an alternative.

In the PFC3D models, the length of each crack (bond breakage) is estimated to be the average of the diameters of the two particles forming that crack. Assuming a circular surface for all the cracks, the area of each crack can be calculated having its diameter. A damage parameter based on the crack surface area is defined in this study as following:

$$Damage(\%) = \frac{\text{total observed crack surface}}{\text{total possible crack surface}} \times 100 \approx \frac{\text{total observed crack surface}}{(\text{No. of contacts}) \times \frac{\pi D_{ave.}^2}{4}} \times 100 \quad (9)$$

The total possible crack surface has been calculated using a simple algorithm by going through all the contacts and summing up the contact area having average diameter of their forming particles. However, it could also be estimated having the average diameter of particles in each specimen,  $D_{ave}$ .

In order to provide a platform for comparison between the amounts of damage in each type of rock, the resolution (or in other words, the number of contacts in each specimen) was kept constant for all the specimens whose properties are listed in Table 2. Therefore, the total possible crack surface area has been equal to 426 mm for all the PFC3D specimens. It is worth mentioning that since the damage parameter is defined based on the crack “surface area”, it is not dependent on the size of particles and thus it was not necessary to repeat the tests with different size of particles as it would be if the “crack length” was used instead of the crack surface area.

As was discussed previously, the PFC3D magnitudes are somehow overestimated even for the algorithm used in present research that works based on changes in strain energy. Therefore,

instead of correlating the damage parameter to PFC3D acoustic emission energies, it would be more reasonable to first correlate it to the consumed energies by PFC3D specimens and then assuming  $W_{PFC3D} = W_{UCT}$ , find the correlation between the damage parameter and real energies. For this purpose, variations of the damage parameter versus total consumed energy by PFC3D specimens are plotted in Figure 9.

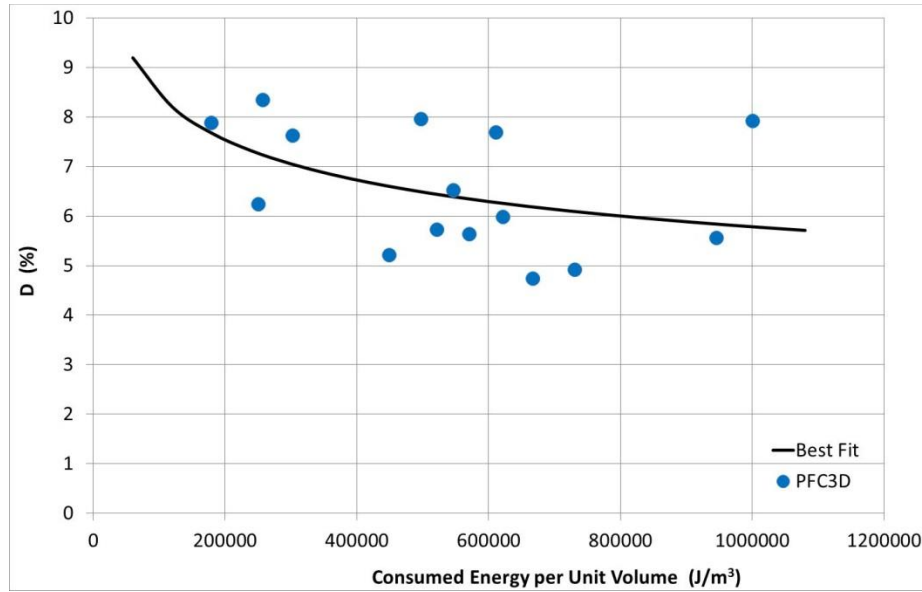


**Figure 9: Variations of damage parameter versus the consumed energy per unit volume of PFC3D models**

The best fitted line in this Figure can be represented by Equation (10) (adjusted  $R^2=0.12$ ):

$$D(\%) = 56.31 \times W_{PFC3D}^{-0.16} \quad (10)$$

Assuming  $W_{PFC3D} = W_{UCT}$  and therefore substituting  $W_{UCT}$  from Equation (5) with  $W_{PFC3D}$  in Equation (10), a correlation between the real released AE energy per volume and damage parameter is obtained as:

$$D(\%) = 0.73 \times E_{UCT}^{-0.16} \quad (11)$$

For simplicity, Figure 10 illustrates the variations of damage parameter based on Equation (11).

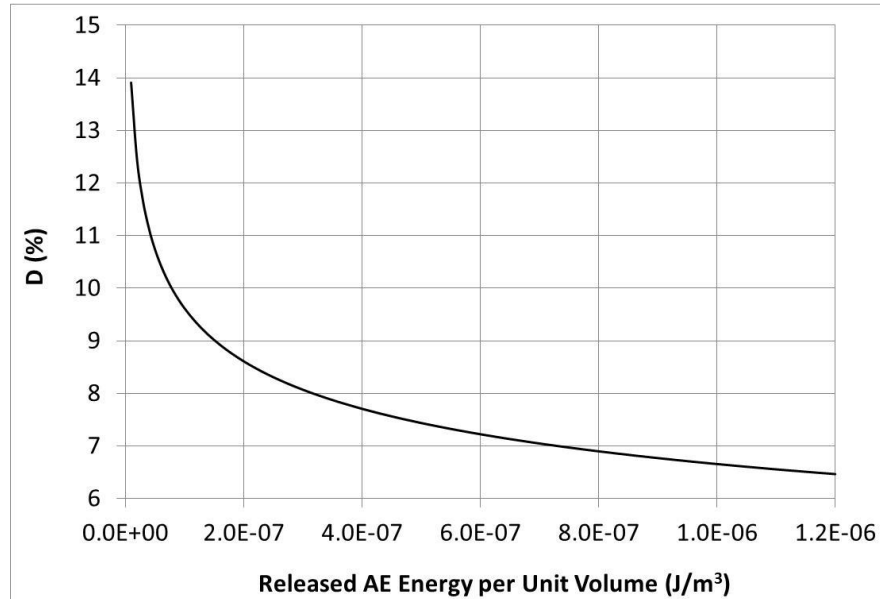


**Figure 10: Variations of damage parameter versus the released AE energy per volume of rock**

As can be observed in this Figure, the greater amounts of released AE energy that obviously correspond to greater amounts of consumed energy belonging to stronger rocks would result in less amount of damage meaning a more localized damage.

## 5. Discussion

As mentioned before, the tests have been conducted by CANMET using stress-controlled mode that unlike strain-controlled mode, doesn't allow obtaining the post peak stress-strain curve. Therefore, all the analyses on laboratory data are based on stress-strain curves and AE data recorded until peak strength. The controversy of this approach is explained using Figure 11 that is compiled from literature. As can be observed in this Figure, there is a general difference between the appearance of AE events with regard to the peak strength in granites (a, b and c) compared to weaker rocks (d, e and f). In the granite rocks, the highest AE activity corresponds to almost pre-peak or peak strength whereas in weaker rocks, the highest AE activity is observed in the post-peak part of the curve. This can be explained considering the greater ductility of weaker rocks that results in larger plastic deformations and higher excess energy in the post peak region.

A comparison between this Figure and Figure 6 suggests that if the post-peak response was recorded in the lab, a larger total AE energy would have been recorded for the weak rocks and the data points belonging to them in Figure 6 would have been somehow shifted up. Therefore, in order to study the AE behavior (at least in weak rocks), using the strain-controlled mode seems more appropriate.

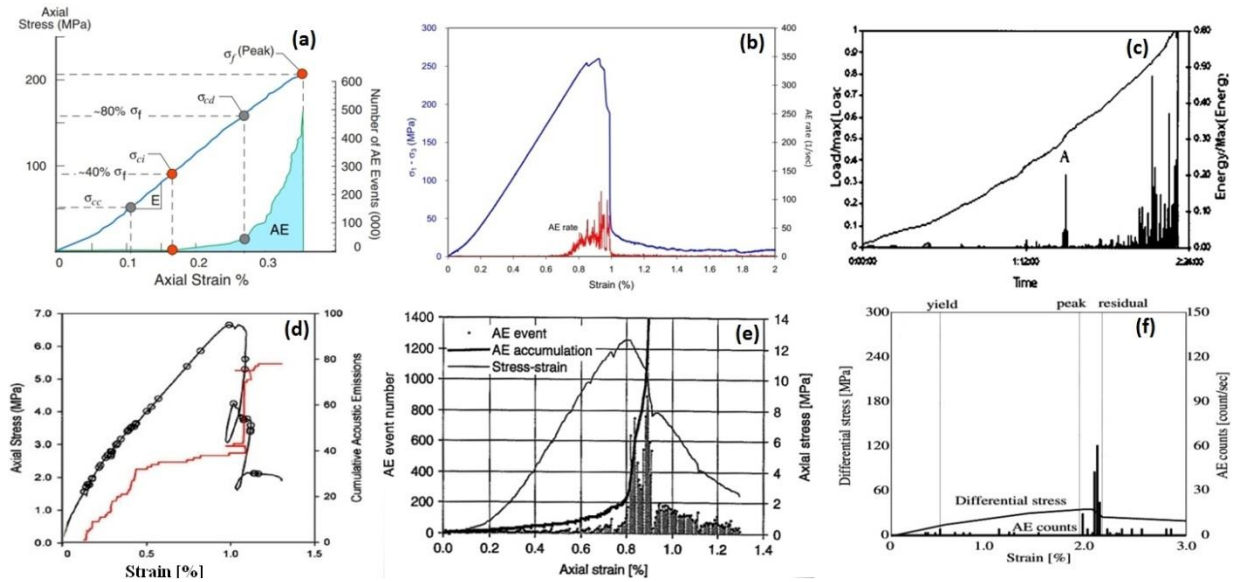


**Figure 11: A comparison between the MS response of brittle and ductile rocks. (a) Lac Du Bonnet granite modified after [Martin, 1993]. (b) Kannagawa powerhouse granite [Cai et al., 2008]. (c) Hong Kong granite (point A was believed to be due cracking within grains) [Liu et al., 2000]. (d) Opalinus clay (AE events are shown by circles. The red line shows the cumulative AE events) [Amann et al., 2011] (e) Soft tuff rock called “Tage tuff” [Mori et al., 2007]. (f) Soft sedimentary rocks obtained from Horonobe URL [Mito et al., 2007]**

Also, the initial non-linear part in stress-strain response of rocks is believed to be due to closure of pre-existing microcracks and thus, the origin of AE events in this part, recorded in laboratory, is due to crack closure too. Therefore, conceptually the damage parameter in Equation (11) which is based on crack surface area needs to be modified to account for this phenomenon. However, as can be observed in Figure 11, the amount of AE activity in this part is very small compared to the rest of emissions and thus this modification is not considered in this work.

In order to get realistic AE magnitudes due to bond breakages (cracking) in PFC3D models, a modified version of Gutenberg-Richter formula was proposed in this research. The reason why magnitudes have been overestimated by the PFC models could be due to contribution of many factors as explained below:

1- In reality, there is breakage of asperities and formation of gouge material at the source causing dissipation of the AE waves and smaller magnitudes while in the PFC3D model, there are no such things and thus the recorded energies are probably too efficient.

2- In PFC3D models, bond breakages and consequently stress drops are instantaneous causing too much energy release while in reality there is a gradual weakening involved between the bonds. It is believed that using a softening contact model in future may solve this problem.

3- Due to practical limitations, not all the AE events are recorded in a lab experiment while PFC records all the events as they occur.

4- The PFC3D magnitudes are calculated either by using Equation (2) and changes in strain energy or by using  $M_w = (2/3)\log M_0 - 6$  and integrating around the forces surrounding each bond breakage [Hazzard & Young, 2002] as discussed in section 3.1. However, both these formulas have been originally proposed for real earthquake events with shear nature along a fault. Although in PFC, the parallel bonds can break either in tension or shear, it is important to differentiate between the events due to such shear cracks in a compressive stress regime with slip induced events along pre-existing weak planes. The events along pre-existing weak planes are governed by a “stick-slip” process and have been studied by the authors in a separate work [Khazaei et al., 2015].

5- It is known that calibration of PFC models for uniaxial compressive strength would result in overestimation of the tensile strength of the specimens. An old solution would be to use clumps as suggested by [Cho et al., 2007] or to use flat jointed model as suggested by [Potyondy, 2012]. Although the strength of micro parameters in PFC does not linearly correspond to the macro strength, it may be the case that micro tensile strengths are greater than what they should be in reality and thus their breakage yields in release of a higher energy resulting in greater AE magnitudes.

How much any of these factors contribute in larger magnitudes is not clearly known. Also, we do acknowledge the fact that correlations proposed in the present research are based on curve fittings with low R2 values indicating a large discrepancy amongst the data point. One reason may be that a realistic level of heterogeneity that is reflected in the shape of particles and

definitely varies from rock to rock was not well modeled by using spherical particles for all the numerical specimens studied in present research. However, it is suggested that using Equation (8) for calculation of PFC3D magnitudes is a reasonable approach for getting realistic events and therefore in practice, the plots and correlations proposed in the present research are applicable provided the assumption that the recorded events have a crack nature within the intact rock could be justified. In other words, there has to be no weak planes in the space where AE events are located to generate slip induced events or their contribution in the AE events is negligible. Also, since the energy release per unit volume has been used in this research, in practice, a judgment has to be made on the choice of appropriate “volume” to result in reasonable conclusions.

## **6. Conclusion**

Acoustic emission response of intact rocks was studied in this research by investigating the recorded AE energies from uniaxial compression tests on 73 specimens of different rock types with UCS values ranging from 3 to 195 MPa reported by CANMET.

The b-values for the lab data were in the range of 0.2-1 with a small decrease for stronger rocks. This agrees well with the fact that larger magnitude events are usually expected for harder rocks. Also, studying the maximum energy recorded for each test showed that the largest magnitudes recorded for all the specimens varied between -9 and -10. This is something to consider especially when using uniaxial compression tests to characterize the AE behavior of rocks in applications where larger magnitude events in the order of, for instance, -1 to -3 have been observed in the field. Also, literature review suggests that in general, the highest level of AE activity appears at pre-peak and post-peak part of stress-strain curve for brittle and ductile rocks, respectively.

According to Figure 3, the rocks with smaller UCS are the more ductile ones with smaller Young's moduli and therefore the fact that they are less emissive compared to strong rocks could be easily understood from Figure 1. However, using the lab data in Figure 6, it was observed that a linear correlation does exist between the total recorded acoustic energies versus total consumed energy by each specimen and therefore Equation (5) suggests that the total released acoustic energy is linearly increased with an increase in the total consumed energy by each intact rock.

In order to study the damage process in more details, discrete element models were also used to study the relation between AE energies and consumed energy by synthetic rock samples. The results confirmed that PFC3D magnitudes are significantly greater than the real values recorded in the lab and therefore, a modification of the Gutenberg-Richter formula was suggested for calculating PFC3D magnitudes due to cracking in a compressive stress regime.

A quantitative study of the crack length/surface was not possible in the present research due to lack of data. However, using discrete element models, a damage parameter was proposed based on the observed crack surface area during the failure process and total possible crack area based on the size of particles. Although the correlation between the crack surface data and energies obtained by PFC3D was poor and more investigation would be required, in practice, if real knowledge of aggregate size distribution is available, an estimate of how much crack surface has been developed could be obtained using the recorded AE energies and proposed charts in this paper.

Finally, the analyses presented in this research are based on the assumption that the failure process of all intact rocks studied in the paper involves the same pattern of compression induced cracks growing, coalescing and forming shear bands leading to the rupture. Therefore, the charts and correlations would be useful in cases where there is enough evidence to believe the recorded AE events are due to cracking within the intact rock as opposed to the events with stick-slip nature that are likely along pre-existing weak planes.

## **Acknowledgement**

The authors are grateful to Tom Lam, Denis Labrie, Dr. Raymond Durrheim, Ehsan Ghazvinian and Ted Anderson for their valuable help in providing us with the lab data. Also, we would like to thank the staff members of Mistras Group especially Ron Miller, Dr. Adrian Pollock and Shawn Jeffered for their help on details of AEWin software and energy analyses. The constructive comments by Dr. Derek Martin and anonymous reviewer on the paper are appreciated.

## References

- Amann, F., Button, E. A., Evans, K. F., Gischig, V. S., & Blümel, M. (2011). Experimental study of the brittle behavior of clay shale in rapid unconfined compression. *Rock Mechanics and Rock Engineering*, 44(4), 415–430.
- ASTM. (2005). ASTM D5878 - Standard Guides for Using Rock-Mass Classification Systems for Engineering Purposes. In *Annual Book of ASTM Standards Vol. 04.08*.
- ASTM. (2007). Standard Test Method for Compressive Strength and Elastic Moduli of Intact Rock Core Specimens under Varying States of Stress and Temperatures. In *Annual Book of ASTM Standards*.
- Brown, E. T. (1981). ISRM suggested methods. Rock characterization testing and monitoring. Pergamon Press, Oxford.
- Cai, M. (2010). Practical estimates of tensile strength and Hoek–Brown strength parameter  $m_i$  of brittle rocks. *Rock Mechanics and Rock Engineering*, 43(2), 167–184.
- Cai, M., Kaiser, P. K., Tasaka, Y., Kurose, H., Minami, M., & Maejima, T. (2008). Numerical Simulation of Acoustic Emission in Large-scale Underground Excavations. In *The 42nd US Rock Mechanics Symposium (USRMS)*. American Rock Mechanics Association.
- Cai, M., Morioka, H., Kaiser, P. K., Tasaka, Y., Kurose, H., Minami, M., & Maejima, T. (2007). Back-analysis of rock mass strength parameters using AE monitoring data. *International Journal of Rock Mechanics and Mining Sciences*, 44(4), 538–549.
- Cho, N., Martin, C. D., & Sego, D. C. (2007). A clumped particle model for rock. *International Journal of Rock Mechanics and Mining Sciences*, 44(7), 997–1010. doi:10.1016/j.ijrmms.2007.02.002
- Cox, S. J. D., & Meredith, P. G. (1993). Microcrack formation and material softening in rock measured by monitoring acoustic emissions. In *International journal of rock mechanics and mining sciences & geomechanics abstracts* (Vol. 30, pp. 11–24). Elsevier.
- Damjanac, B. (2010). *Energy release due to fracturing in BPM*. Minneapolis, MN, USA.
- Eberhardt, E., Stead, D., & Stimpson, B. (1999). Quantifying progressive pre-peak brittle fracture damage in rock during uniaxial compression. *International Journal of Rock Mechanics and Mining Sciences*, 36(3), 361–380. doi:10.1016/S0148-9062(99)00019-4
- Elaqra, H., Godin, N., Peix, G., R'Mili, M., & Fantozzi, G. (2007). Damage evolution analysis in mortar, during compressive loading using acoustic emission and X-ray tomography:

- Effects of the sand/cement ratio. *Cement and Concrete Research*, 37(5), 703–713.  
doi:10.1016/j.cemconres.2007.02.008
- Fairhurst, C. (2013). Fractures and Fracturing: Hydraulic Fracturing in Jointed Rock. *ISRM International Conference for Effective and Sustainable Hydraulic Fracturing*. Retrieved from <https://www.onepetro.org/conference-paper/ISRM-ICHF-2013-012>
- Fujii, H., Saito, Y., Tanaka, M., Machijima, Y., & Mori, T. (2009). The AE Characteristic in Hard rock and Soft Rock Specimens of Compression Failure Using Optical Type AE Sensor (FOD). *NATIONAL CONFERENCE ON ACOUSTICAL EMISSION*, (17), 99–102. Retrieved from <https://getinfo.de/app/VI-4-The-AE-Characteristic-in-Hard-rock-and-Soft/id/BLCP%3ACN076722467>
- Ganne, P., Vervoort, A., & Wevers, M. (2007). Quantification of pre-peak brittle damage: Correlation between acoustic emission and observed micro-fracturing. *International Journal of Rock Mechanics and Mining Sciences*, 44(5), 720–729.  
doi:10.1016/j.ijrmms.2006.11.003
- Gorski, B., Anderson, T., & Conlon, T. (2009a). *Labratory Geomechanical Strength Testing of DGR-1 & DGR-2 Core*. Retrieved from DGR Site Characterization Document, Intra Engineering Project 06-219
- Gorski, B., Anderson, T., & Conlon, T. (2009b). *Labratory Geomechanical Strength Testing of DGR-3 & DGR-4 Core*.
- Griffith, A. A. (1921). The phenomena of rupture and flow in solids. *Philosophical Transactions of the Royal Society of london. Series A, Containing Papers of a Mathematical or Physical Character*, 221, 163–198.
- Griffith, A. A., Biezeno, C. B., & Burgers, J. M. (1997). The theory of rupture. *SPIE MILESTONE SERIES MS*, 137, 96–104.
- Gutenberg, B. u., & Richter, C. F. (1954). *Seismicity of the earth and related phenomena. Princeton (NJ)*.
- Hall, S. A., De Sanctis, F., & Viggiani, G. (2006). Monitoring fracture propagation in a soft rock (Neapolitan Tuff) using acoustic emissions and digital images. *Pure and Applied Geophysics*, 163(10), 2171–2204.
- Harrison, J. P., & Hudson, J. A. (2000). *Engineering rock mechanics-an introduction to the principles*. Elsevier.
- Hazzard, J., & Damjanac, B. (2013). Further investigations of microseismicity in bonded particle models.

- Hazzard, J., & Young, R. P. (2000). Simulating acoustic emissions in bonded-particle models of rock. *International Journal of Rock Mechanics and Mining Sciences*, 37(5), 867–872. Retrieved from <http://cat.inist.fr/?aModele=afficheN&cpsid=1419981>
- Hazzard, J., & Young, R. P. (2002). Moment tensors and micromechanical models. *Tectonophysics*, 356(1), 181–197.
- Hazzard, J., & Young, R. P. (2004). Dynamic modelling of induced seismicity. *International Journal of Rock Mechanics and Mining Sciences*, 41(8), 1365–1376.
- Hill, R., Dixon, N., & Kavanagh, J. (1998). Monitoring deformation of soil slopes using AE: Case histories. *Series on Rock and Soil Mechanics*, 21, 381–400.
- Itasca, C. G. (1999). PFC 3D-User manual. *Itasca Consulting Group, Minneapolis*.
- Khazaei, C., Hazzard, J., & Chalaturnyk, R. J. (2015). Discrete element modeling of stick-slip instability and induced microseismicity. *Pure and Applied Geophysics*. doi:10.1007/s00024-015-1036-7
- Kishi, T., Ohtsu, M., & Yuyama, S. (2000). *Acoustic emission-beyond the millennium*. Elsevier.
- Koerner, R. M., & Lord, A. E. (1984). *Spill alert device for earth dam failure warning*. Cincinnati, OH: U.S. Environmental Protection Agency, Municipal Environmental Research Laboratory: Center for Environmental Research Information [distributor].
- Koerner, R. M., McCabe, W. M., & Lord, A. E. (1977). Acoustic emission behavior of cohesive soils. *Journal of the Geotechnical Engineering Division*, 103(8), 837–850.
- Koerner, R. M., McCabe, W. M., & Lord Jr, A. E. (1981). Acoustic emission behavior and monitoring of soils. In *Acoustic emissions in geotechnical engineering practice: a symposium* (p. 93). ASTM International.
- Lam, T., Martin, D., & McCreath, D. (2007). Characterising the geomechanics properties of the sedimentary rocks for the DGR excavations. In *Canadian Geotechnical Conference, Ottawa*.
- Lavrov, A., Vervoort, A., Filimonov, Y., Wevers, M., & Mertens, J. (2002). Acoustic emission in host-rock material for radioactive waste disposal: comparison between clay and rock salt. *Bulletin of Engineering Geology and the Environment*, 61(4), 379–387. doi:10.1007/s10064-002-0160-7
- Liu, H., Lee, P., Tusi, Y., & Tham, L. (2000). Acoustic emission behavior of brittle rocks under uniaxial compression. In *SEM IX International Congress*. Florida.

- Lockner, D. A. (1993). The role of acoustic emission in the study of rock fracture. *International Journal of Rock Mechanics and Mining Sciences & Geomechanics Abstracts*, 30(7), 883–899. doi:10.1016/0148-9062(93)90041-B
- Lockner, D. A., Byerlee, J., Kuksenko, V., Ponomarev, A., & Sidorin, A. (1991). Quasi-static fault growth and shear fracture energy in granite. *Nature*, 350(6313), 39–42.
- Manthei, G., Eisenbltter, J., & Spies, T. (2000). *Acoustic Emission in Rock Mechanics Studies in Acoustic Emission-Beyond the Millennium*. Elsevier, London.
- Martin, C. D. (1993). *The strength of massive Lac du Bonnet granite around underground openings*. Retrieved from <http://mspace.lib.umanitoba.ca/jspui/handle/1993/9785>
- Martin, C. D., & Chandler, N. A. (1994). The progressive fracture of Lac du Bonnet granite. In *International Journal of Rock Mechanics and Mining Sciences & Geomechanics Abstracts* (Vol. 31, pp. 643–659). Elsevier.
- Mito, Y., Chang, C. S., Aoki, K., Matsui, H., Niunoya, S., & Minami, M. (2007). Evaluation of Fracturing Process of Soft Rocks At Great Depth By AE Measurement And DEM Simulation. In *11th ISRM Congress*. International Society for Rock Mechanics.
- Mori, T., Nakajima, M., Iwano, K., Tanaka, M., Kikuyama, S., & Machijima, Y. (2007). Application of the fiber optical oscillation sensor to AE measurement at the rock compression test. In *11th Congress of the International Society for Rock Mechanics* (pp. 1101–1104).
- Niandou, H., Shao, J. F., Henry, J. P., & Fourmaintraux, D. (1997). Laboratory investigation of the mechanical behaviour of Tournemire shale. *International Journal of Rock Mechanics and Mining Sciences*, 34(1), 3–16. doi:10.1016/S1365-1609(97)80029-9
- Ohnaka, M., & Mogi, K. (1982). Frequency characteristics of acoustic emission in rocks under uniaxial compression and its relation to the fracturing process to failure. *Journal of Geophysical Research*, 87(B5), 3873. doi:10.1029/JB087iB05p03873
- Pollock, A. A. (2013). AE signal features: energy, signal strength, absolute energy and RMS (Rev. 1.2). *Mistras Group INC - Technical Note 103-22-9/11*, 3.
- Potyondy, D. O. (2012). A Flat-Jointed Bonded-Particle Material For Hard Rock. *46th U.S. Rock Mechanics/Geomechanics Symposium*. Retrieved from <https://www.onepetro.org/conference-paper/ARMA-2012-501>
- Potyondy, D. O., & Cundall, P. A. (2004). A bonded-particle model for rock. *International Journal of Rock Mechanics and Mining Sciences*, 41(8), 1329–1364. doi:10.1016/j.ijrmms.2004.09.011

- Přikryl, R., Lokajíček, T., Li, C., & Rudajev, V. (2003). Acoustic emission characteristics and failure of uniaxially stressed granitic rocks: the effect of rock fabric. *Rock Mechanics and Rock Engineering*, 36(4), 255–270.
- Reches, Z., & Lockner, D. A. (1994). Nucleation and growth of faults in brittle rocks. *Journal of Geophysical Research: Solid Earth (1978–2012)*, 99(B9), 18159–18173.
- Scholz, C. H. (1968). Microfracturing and the inelastic deformation of rock in compression. *Journal of Geophysical Research*, 73(4), 1417–1432. doi:10.1029/JB073i004p01417
- Scholz, C. H. (2002). *The mechanics of earthquakes and faulting*. Cambridge university press.
- Sellers, E. J., Kataka, M. O., & Linzer, L. M. (2003). Source parameters of acoustic emission events and scaling with mining- induced seismicity. *Journal of Geophysical Research: Solid Earth (1978–2012)*, 108(B9).
- Seto, M., Utagawa, M., & Katsuyama, K. (2002). Some fundamental studies on the AE method and its application to in-situ stress measurements in Japan. In *Proc. 5th Int. Workshop on the Application of Geophysics in Rock Engineering, Toronto, Canada, (2002.)* (Vol. 67, p. 71).
- Sondergeld, C. H., & Estey, L. H. (1981). Acoustic emission study of microfracturing during the cyclic loading of Westerly granite. *Journal of Geophysical Research: Solid Earth (1978–2012)*, 86(B4), 2915–2924.
- Suzuki, T., Ogata, H., Takada, R., Aoki, M., & Ohtsu, M. (2010). Use of acoustic emission and X-ray computed tomography for damage evaluation of freeze-thawed concrete. *Construction and Building Materials*, 24(12), 2347–2352. doi:10.1016/j.conbuildmat.2010.05.005
- Thoeny, R., Amann, F., & Button, E. (2010). Ground conditions and the relationship to ground behavior—a new mine-by project in Opalinus clay at Mont Terri Rock Laboratory. *Rock Mechanics and Environmental Engineering*, (Zhao J, Labiouse V, Dudt J-P, Mathier J-F (eds)), 775–778.
- Valès, F., Nguyen Minh, D., Gharbi, H., & Rejeb, A. (2004). Experimental study of the influence of the degree of saturation on physical and mechanical properties in Tournemire shale (France). *Applied Clay Science*, 26(1-4), 197–207. doi:10.1016/j.clay.2003.12.032
- Watanabe, K., Niwa, J., Iwanami, M., & Yokota, H. (2004). Localized failure of concrete in compression identified by AE method. *3rd Kumamoto International Workshop on Fracture, Acoustic Emission and NDE in Concrete (KIFA-3)*, 18(3), 189–196. doi:10.1016/j.conbuildmat.2003.10.008

Young, R. P. ... Dedecker, F. (2005). Seismic Validation of 3-D Thermo-Mechanical Models for the Prediction of the Rock Damage around Radioactive Waste Packages in Geological Repositories-SAFETI. *Final Report, European Commission Nuclear Science and Technology*.

Yukalov, V. I., Moura, A., & Nechad, H. (2004). Self-similar law of energy release before materials fracture. *Journal of the Mechanics and Physics of Solids*, 52(2), 453–465. doi:10.1016/S0022-5096(03)00088-7

Zang, A., Wagner, F. C., Stanchits, S., Janssen, C., & Dresen, G. (2000). Fracture process zone in granite. *Journal of Geophysical Research: Solid Earth (1978–2012)*, 105(B10), 23651–23661.